 CMES, vol.116, no.2, pp.263-279, 2018

Mechanical Strength and Structural Basis of β_2 Integrin to Mediate Neutrophil Accumulation on Liver Sinusoidal Endothelial Cells: A Study Using Atomic Force Microscopy and Molecular Dynamics Simulations

Ning Li[1, 2, 3], Xiao Zhang[1, 2], Peiwen Li[1, 2], Hao Yang[1, 2], Chunfang Tong[1, 2], Shouqin Lü[1, 2], Yan Zhang[1, 2], Zhiyi Ye[3], Jun Pan[3, *] and Mian Long[1, 2, *]

Abstract: Neutrophil (PMN) accumulation on liver sinusoidal endothelial cells (LSECs) is crucial to pathogen clearance and tissue damage in the liver sinusoids and controlled by a series of adhesion molecules expressed on the surface of PMNs and LSECs. The role of lymphocyte function-associated antigen-1 (LFA-1) and macrophage-1 antigen (Mac-1) in this process is still contentious. Here we compared the dynamic force spectra of the binding of β_2 integrin to intercellular adhesion molecule-1 (ICAM-1) on LSECs using atomic force microscopy (AFM) and performed free and steered molecular dynamics (MD) simulations to analyze their structural bases of LFA-1- or Mac-1-I-domain and ICAM-1-D1 or D3 pair in their force spectra. Our AFM data suggest that the mechanical strength of LFA-1-ICAM-1 bond is significantly stronger than that of Mac-1-ICAM-1 bond, implying a dominate role for LFA-1 to mediate PMN adhesion under shear flow. MD simulations indicated that spontaneous dissociation of Mac-1-I-domain *vs.* ICAM-D3-domain is slower with the stronger interaction energy than that for LFA-1 I-domain *vs.* ICAM-D1-domain and that the rupture force for Mac-1 is lower than that for LFA-1, which are in qualitative agreement with the above experimental observations. These data indicate that the biomechanical features of LFA-1 and Mac-1 to mediate PMN adhesion on LSECs *in vitro* are similar with those in other tissues like cerebrovascular endothelium, while Mac-1-mediated PMN recruitment in liver sinusoids may stem from the slow blood flow *in vivo*. These findings further the understandings of PMN recruitment under shear flow in liver sinusoids.

Keywords: Liver sinusoidal endothelial cells, neutrophils, β_2 integrin, shear flow, mechanical strength.

[1] Center of Biomechanics and Bioengineering, Key Laboratory of Microgravity (National Microgravity Laboratory), and Beijing Key Laboratory of Engineered Construction and Mechanobiology, Institute of Mechanics, Chinese Academy of Sciences, No. 15 Beisihuanxi Road, Beijing, 100190, China.

[2] School of Engineering Sciences, University of Chinese Academy of Sciences, No.19(A) Yuquan Road, Shijingshan District, Beijing, 100049, China.

[3] Key Laboratory of Biorheological Science and Technology, Chongqing University, Ministry of Education, No.174 Shazhengjie, Shapingba, Chongqing, 400044, China.

[*] Corresponding Author: Mian Long. E-mail: mlong@imech.ac.cn; Jun Pan. E-mail: panj@cqu.edu.cn.

1 Introduction

Liver sinusoidal endothelial cells (LSECs) are highly specialized endothelial cells which form the wall of the liver sinusoids and the interface between the bloodstream and the liver parenchyma [Vollmar and Menger (2009); Xu, Wang, Zou et al. (2017); Zapotoczny, Szafranska, Kus et al. (2017)]. LSECs mediate the exchange of oxygen, nutrients, lipids, and proteins between hepatic sinusoids and hepatocytes through small fenestrae. These fenestrae are non-diaphragmed pores with a diameter of 50-150 nm and organized in clusters termed sieve plates [Yamasaki, Ikeda, Nakatani et al. (1999); Poisson, Lemoinne, Boulanger et al. (2017)]. Liver injury can cause LSECs to lose their fenestrae and large gaps (0.3-2 μm) formation, which mainly promotes the interactions between LSECs and circulating leukocytes or tumor cells under biochemical and biomechanical stimuli [Braet, Shleper, Paizi et al. (2004); Ito, Abril, Bethea et al. (2006); Sanabria and Dong (2018)].

LSECs also serve as an important barrier in the innate immune responses, providing the first line of defense against intestinal pathogens and toxins. Polymorphonuclear leukocyte (neutrophil, PMN) recruitment in the liver sinusoids is widely observed in almost all liver diseases and contributes to pathogen clearance or tissue damage [Ramaiah and Jaeschke (2007); Heymann and Tacke (2016)]. PMN accumulation within sinusoids and their extravasation into the parenchyma is controlled by a series of adhesion molecules expressed on the surface of PMNs and LSECs. Lymphocyte function associated antigen-1 (LFA-1, $\alpha_L\beta_2$, CD11a/CD18) and macrophage-1 antigen (Mac-1, $\alpha_M\beta_2$, CD11b/CD18) are two β_2 integrins expressed on PMNs and mediate PMN slow rolling, firm adhesion, intraluminal crawling and transendothelial migration in postcapillary venules [Ley, Laudanna, Cybulsky et al. (2007); Lyck and Enzmann (2015); Shi, Wang and Liu (2016)]. However, the role of LFA-1 and Mac-1 in PMN recruitment within liver sinusoids is still controversial. Upon intravital microscopic studies, PMN accumulation within the sinusoids during lipopolysaccharide (LPS)-induced systemic inflammation does not require β_2 integrins, while Mac-1, but not LFA-1, does mediate PMN recruitment during sterile injury, local virus infection or fMLF stimulation [McDonald, McAvoy, Lam et al. (2008); Menezes, Lee, Zhou et al. (2009); McDonald, Pittman, Menezes et al. (2010); Jenne, Wong, Zemp et al. (2013)]. In contrast, LFA-1 dominates fMLF-activated PMN adhesion while Mac-1 decelerates PMN crawling on tumor necrosis factor-α (TNF-α)-stimulated LSEC monolayer under shear flow *in vitro* [Yang, Li, Du et al. (2017)]. Thus, it is crucial to elaborate the respective contributions of the two β_2 integrins in PMN hepatic recruitment.

One way to elucidate the underlying mechanisms is to quantify the mechanical strength of β_2 integrin-ligand bonds because the bond strength defines how strong the interactions between PMNs and LSECs could be under blood flow [Zhang, Wojcikiewicz and Moy (2002); Lü, Ye, Zhu et al. (2006); Zhang, Sun, Lü et al. (2008); Swartjes and Veeregowda (2015); Mittal and Dwivedi (2017); Li, Yang, Wang et al. (2018)]. Our previous work applied a flow chamber assay to compare the capabilities of LFA-1- or Mac-1-mediated PMN adhesion on LSECs to resist shear flow and revealed the higher adhesion strength through LFA-1 than Mac-1 at cellular level [Yang, Li, Du et al. (2017)]. In the current study, we quantified the dynamic force spectra of the binding of β_2 integrin to intercellular adhesion molecule-1 (ICAM-1) on LSECs at molecular level

using atomic force microscopy (AFM). Force dependence of bond lifetimes, tissue specificity and structural differences of LFA-1- or Mac-1-ICAM-1 binding were also discussed. These findings provide an insight in understanding PMN recruitment under shear flow in liver sinusoids.

2. Materials and methods

2.1 Antibodies and reagents

Recombinant mouse LFA-1 (CD11a/CD18), Mac-1 (CD11b/CD18) and TNF-α were purchased from R&D Systems (Minneapolis, MN). FITC-conjugated rat-anti-mouse CD146 monoclonal antibodies (mAbs) for cytometry sorting were from Miltenyi Biotec (Bergisch Gladbach, Germany). Rat anti-mouse blocking mAbs against CD11a (M17/4) and CD11b (M1/70), and isotype control (RTK2758, RTK4530) mAbs were all from Biolegend (San Diego, CA). Bovine serum albumin (BSA), fMLF, glutaraldehyde and $MnCl_2$ were obtained from Sigma-Aldrich (St Louis, MO).

2.2 Cells

LSECs were isolated from 8-12 week-old C57BL/6 male mice obtained from Vital River Laboratories (Beijing, China) as previously described [Du, Li, Yang et al. (2017); Yang, Li, Du et al. (2017); Li, Yang, Wang et al. (2018)] after approval by the Institutional Animal and Medicine Ethical Committee (IAMEC) at the Institute of Mechanics, Chinese Academy of Sciences. Briefly, LSECs were isolated by a two-step collagenase perfusion of whole liver to digest liver tissues, a low speed centrifugation to separate fraction of hepatocytes, a density gradient centrifugation of the nonparenchymal cells on 11.7% to 17.6% Optiprep^{TM} solution (Axis-Shield, Dundee, Scotland) gradients, and a cytometry sorting with CD146 by FACS Aria III (BD Biosciences, San Jose, CA). Isolated LSECs and mice brain microvascular endothelial cell line bEnd.3, purchased from American Type Culture Collection (Manassas, VA), were cultured in 35 mm culture dishes with Endothelial Cell Medium (ECM, Sciencell Research Laboratories, Carlsbad, CA) at 37°C with 5% CO_2. LSECs and bEnd.3 cells were cultured for 48 h and stimulated with 100 ng/ml TNF-α or 1 μg/ml LPS for 12 h before use.

2.3 AFM imaging

AFM imaging was conducted at room temperature (RT) on a BioScope Catalyst AFM (Bruker Corporation, Santa Barbara, CA). All measurements were performed in Dulbecco's phosphate-buffered saline (DPBS) using soft silicon nitride cantilevers (MLCT-C, Bruker, Santa Barbara, CA) with pyramidal tips and a spring constant of 0.01 N/m. LSECs cultured for 48 h in dish were fixed with 1% glutaraldehyde at RT for 15 min. After being washed 3 times with DPBS, the samples were placed on the AFM stage and scanned with contact mode. Whole cell imaging was performed within a 50×50 μm scanning area at 512×512 pixels and 0.5 Hz scan frequency. High-magnification images were obtained using the following settings: 16.6×16.6 μm scanning area, 256×256 pixels and 1 Hz frequency.

2.4 Dynamic force spectrum measurements

AFM was also used to measure the rupture force between an ICAM-1-expressing LSEC or a bEnd.3 cell and a β_2-integrin-captured AFM tip [Li, Yang, Wang et al. (2018)]. All force measurements were conducted in Mn^{2+} stimulation buffer (1 mM Mn^{2+} in the presence of Ca^{2+}- and Mg^{2+}-free HBSS containing 0.1% BSA) at RT on a BioScope Catalyst AFM using MLCT-C cantilevers, since it is known that β_2-integrin can be activated by Mn^{2+} [Lu, Shimaoka, Ferzly et al. (2001); Shimaoka, Lu, Salas et al. (2002); Evans, Kinoshita, Simon et al. (2010); Kinoshita, Leung, Simon et al. (2010)]. To prepare the β_2-integrin functionalized AFM cantilevers, the cantilever tips were incubated with 100 μg/ml mouse LFA-1s or Mac-1s for 2 h at 37°C. The cantilevers were then washed with DPBS to remove unbound β_2-integrin and incubated with 1% BSA for 1 h at 37°C to block nonspecific adhesion sites. In some cases, the cantilevers were incubated with 20 μg/ml isotype control or LFA-1/Mac-1 blocking mAbs in DPBS for 1 h at 37°C. The blocking mAbs would bind to the integrins coated on the cantilevers and the unbound antibodies were washed out with DPBS. TNF-α-stimulated LSECs or LPS-activated bEnd.3 cells in a 35 mm-culture dish were incubated with Mn^{2+} stimulation buffer for 1 h before force measurements. After placing the dish onto the AFM stage, a β_2-integrin-coated cantilever tip was repeatedly driven by a piezoelectric translator (PZT) to approach the cell at the rate of 1 μm/s, to make contact at a compressive force of 200 pN for 50 ms to allow reversible bond formation and dissociation, and to retract away to allow the observation of the adhesion event and the measurement of rupture force, if any. The retraction rate of the cantilever was varied from 0.5-8 μm/s to acquire the measurements at different loading rates. The rupture force between the two molecules was derived from the deflection of the AFM cantilever, which was monitored by reflecting a focused laser beam off the back of the cantilever into a quad photodetector (QPD). At least three different cells on each dish were tested for 50 cycles each cell to collect a set of adhesion events and rupture forces. All experiments were repeated at least in triplet. 600~1000 force curves were recorded in each retraction speed. For single molecule data analysis, only the force curves exhibiting a single rupture with signal/noise >3, but not a force plateau, were considered as single force ramp rupture events. Total of >50 single forces at each loading rate (except for LFA-1 *vs.* bEnd.3 at r_f=1363 pN/s, which had 36 forces) were collected. The rupture force of the β_2-integrin-ICAM-1 complex, f, was collected from the peak of the rupture event to zero force. The loading rate, r_f, was determined by first evaluating the slope of the force-displacement curve just before each rupture event and then multiplying this number (pN/nm) by the retraction velocity (nm/s). According to the Bell model [Bell (1978)], the dissociation rate, $k(f)$, is assumed to depend exponentially on applied force is used,

$$k(f) = \frac{1}{\tau(f)} = k^0 \exp\left(\frac{af}{k_B T}\right) \tag{1}$$

where τ is the bond lifetime, k^0 is the equilibrium dissociation rate, k_B is the Boltzmann constant, T is the absolute temperature, and a is a measure of bond compliance width. Under the condition of constant loading rate, the probability density function for the dissociation of a bond at force f is given by Evans et al. [Evans and Ritchie (1997)]:

$$P(f) = k^0 \exp\left(\frac{af}{k_B T}\right) \exp\left\{\frac{k^0 k_B T}{a r_f}\left[1 - \exp\left(\frac{af}{k_B \mathrm{T}}\right)\right]\right\} \tag{2}$$

The average rupture force, <*f*>, follows the so-called dynamic force spectroscopy (DFS) theory [Evans and Ritchie (1997)]:

$$\langle f \rangle = \frac{k_B \mathrm{T}}{a} \ln\left(\frac{a}{k^0 k_B T}\right) + \frac{k_B T}{a} \ln\left(r_f\right) \tag{3}$$

The bond lifetime is transformed directly from the variance of rupture force distribution [Dudko, Hummer and Szabo (2008)]:

$$\tau\left(\langle f \rangle\right) \approx \left[\frac{\pi}{2}\left(\langle f^2 \rangle - \langle f \rangle^2\right)\right]^{1/2} / r_f \tag{4}$$

2.5 Molecular dynamics simulation

Free and steered molecular dynamics (MD) simulations were performed to analyze the structural bases of LFA-1- or Mac-1-I-domain and ICAM-1-D1 or D3 pair in their distinct force spectra. Simulation systems of human ICAM-1 ligated Mac-1 I domain (PDB code: 1JLM) and LFA-1 I domain (PDB code: 1LFA) were built to evaluate the binding strength of the complex with the Ca^{2+} ion in the MIDAS, as previously described [Mao, Lü, Li et al. (2011); Li, Mao, Lü et al. (2013)]. Each simulation system was established by solvating the target molecule(s) into a rectangular water box and neutralized with ~100 mM Na^+ and Cl^- ions. Free MD simulations were conducted firstly using NAMD [Phillips, Braun, Wang et al. (2005)] program with CHARMM22 [MacKerell, Bashford, Bellott et al. (1998)] all-atom force field following the same specific parameters as described before [Lü and Long (2005); Mao, Lü, Li et al. (2011); Li, Mao, Lü et al. (2013)]. Because Mac-1 I domain was unable to bind to the ICAM-1 D3 domain stably in free MD simulations, a 200 pN constant force steered MD simulation was conducted to enforce the binding by pulling one of the oxygen atoms of D229 residue side-chain in ICAM-1 D3 domain to the fixed MIDAS ion in Mac-1 I domain. After being equilibrated via free MD simulations for 20 ns to reach steady states and similar initial structures [Mao, Lü, Li et al. (2011)], steered MD simulations at a constant velocity (*cv*) of 0.01 Å/ps were conducted to unbind the LFA-1- or Mac-1-ICAM-1 complex upon the equilibrated complex. Here the C-terminal C_α atom of LFA-1 or Mac-1 I domain was fixed and the C-terminal C_α atom of ICAM-1 D1 or D3 domain was pulled along the vector from the fixed atom to the pulled end.

The non-covalent interactions between LFA-1/Mac-1 I domain and ICAM-1 D1/D3 domain, as well as the distribution of main binding sites were calculated in equilibration process to estimate the bond strength and zero-force dissociation kinetics. And the rupture force and the interaction energy evolution between Ca^{2+} ion in LFA-1/Mac-1 I domain and key residue E34/D229 in ICAM-1 D1/D3 domain were estimated in *cv*- steered MD dissociation process to evaluate the resisting capability of LFA-1/Mac-1 I domain-ICAM-1

D1/D3 complex to external force. VMD program was used for system building, data analysis and conformation presentation [Humphrey, Dalke and Schulten (1996)].

2.6 Statistical analysis

Data were presented as the mean±SEM. Significant differences between two groups were analyzed by the unpaired two-tailed Student's *t* test or the Mann-Whitney rank sum test, depending on whether the data pass the normality test (Kolmogorov-Smirnov test). For multiple group comparisons, one-way analysis of variance (ANOVA) test followed by a Holm-Sidak test was performed if passing the normality test or using non-parametric Kruskal-Wallis test followed by Dunn's test if not. *P* values less than 0.05 were considered statistically significant.

3 Results

3.1 LSEC identification with AFM

Primary LSECs were isolated from mice livers and cultured in a 35 mm culture dish for 48 h to form an interconnecting monolayer. It is well accepted that the isolated LSECs undergo capillarization and defenestration over time [Juin, Planus, Guillemot et al. (2013); Ford, Jain and Rajagopalan (2015); Poisson, Lemoinne, Boulanger et al. (2017)]. We examined the specific fenestrae of LSECs using AFM imaging in order to confirm if the LSECs were able to remain undifferentiated. The results indicated that LSECs cultured for 48 h were able to form a monolayer and exhibit well-defined fenestrae arranged in sieve plate structures as expected (*arrows* in Fig. 1), displaying the normal and undifferentiated phenotype.

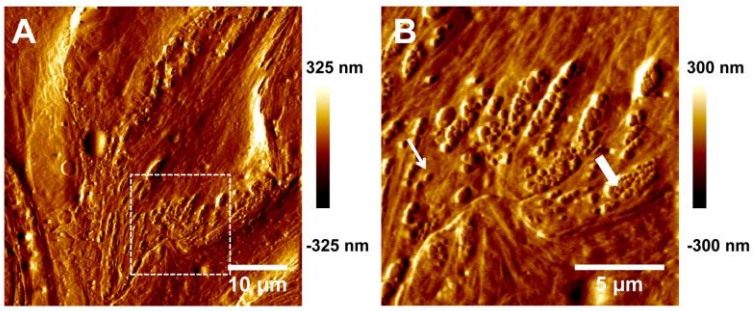

Figure 1: LSECs visualized using AFM in contact mode. (*A-B*) Cell surface morphology (deflection error images) of LSECs cultured for 48 h at low (50×50 µm, 512×512; *A*) or high (16.6×16.6 µm, 256×256; *B*) magnification. The region chosen for further high-magnification imaging was marked in *A*. Thin and thick arrows indicated single fenestration and sieve plates respectively

3.2 Dynamic force spectra for LFA-1 and Mac-1 binding to ICAM-1 on LSECs

We next used AFM to quantify the bond mechanical strength of the interactions between Mn^{2+}-activated β_2 integrins on the cantilever tip and ICAM-1s on TNF-α-stimulated LSECs at molecular level, since the specific rupture force for quiescent molecular pair in

the absence of either Mn^{2+} or TNF-α activation is too weak to detect (data not shown). Fig. 2A presented a series of typical force-displacement curves. Adhesive events and rupture forces were visualized from the middle and lower panels. To achieve the measurement of rupture forces at single-molecule level, the experimental settings such as molecular densities, contact time, and compression force were optimized to result in the binding probability <30%, ensuring a>83% single-bond events [Tees, Waugh and Hammer (2001)]. Here the adhesion probabilities were 22±4% and 13±3% when the LFA-1- or Mac-1-coated tips contacted the LSECs but the adhesion was significantly reduced to 1-5% for tips coated with BSA only or in the presence of LFA-1 or Mac-1 blocking mAbs, demonstrating that the observed adhesion events were mainly mediated by the specific interactions between β_2 integrin-ICAM-1 molecules (Fig. 2B).

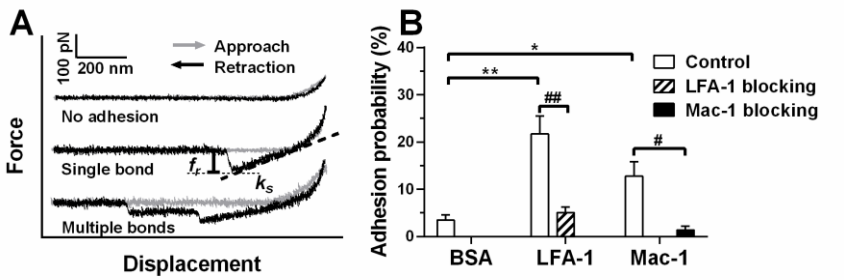

Figure 2: AFM force measurements of Mn^{2+}-activated LFA-1s or Mac-1s on the AFM cantilever tip to ICAM-1s expressed on TNF-α-stimulated LSECs. (*A*) A series of typical force-displacement curves. The LFA-1 or Mac-1-coated AFM tip was driven to approach to (from left to right, grey lines), make contact with, and retract from (from right to left, black lines) the LSECs in the 35 mm culture dish. Adhesion was identified from cantilever deflection and f_r was the rupture force of the β_2 integrin-ICAM-1 bond (middle panel). k_s is the system spring constant derived from the slope of the force-displacement curve. (*B*) Binding specificity. The BSA, LFA-1- or Mac-1-coated tip was pretreated with isotype control (open bars), LFA-1 (cross bars) or Mac-1 blocking (closed bars) mAbs. Adhesion probabilities were measured between the AFM tips and the LSECs at retraction velocity of 1 μm/s. Data were presented as the mean ± SEM of three distinct tips for 5~13 cells in each case. Significant differences among BSA, LFA-1- or Mac-1-coated tips were analyzed with Kruskal-Wallis test followed by Dunn's test and indicated by *, $p<0.05$; **, $p<0.01$. Significant differences between each blocking group and isotype control were analyzed with unpaired two-tailed Student's *t* test and indicated by $^{\#}$, $p<0.05$; $^{\#\#}$, $p<0.01$

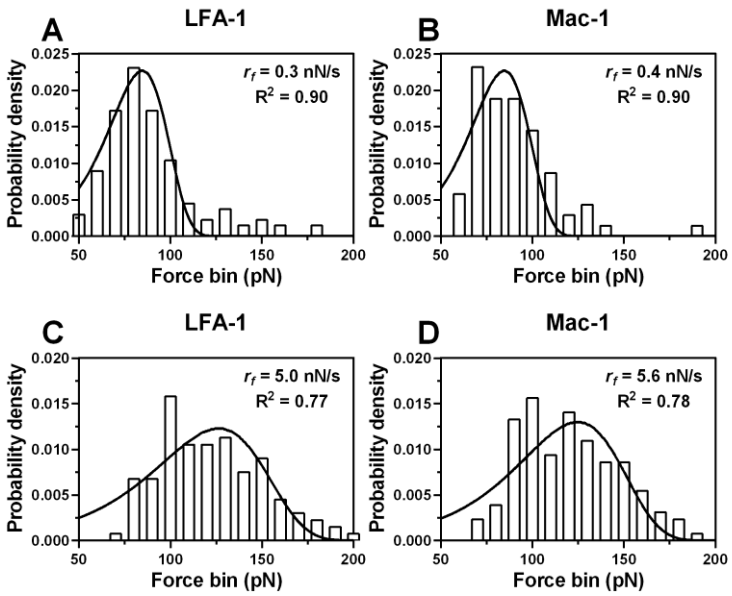

Figure 3: Typical rupture force distributions (*histograms*) of the bindings between Mn^{2+}-activated LFA-1s (*A, C*) or Mac-1s (*B, D*) on the AFM cantilever tip and ICAM-1s expressed on TNF-α-stimulated LSECs acquired at the indicated loading rates. Total 36~144 single-bond rupture force data at each loading rate were collected and analyzed using a force bin of 10 pN. The fitted curves (lines) were obtained using Eq. (2)

Rupture forces of single bonds followed a distribution fitting well with Eq. (2) for both LFA-1 (Figs. 3A, 3C) and Mac-1 (Figs. 3B, 3D) at a given loading rate. The force distribution exhibited a single peak at each loading rate and was shifted toward higher values with increasing loading rates. Both the mean force spectra of LFA-1 and Mac-1 followed a linear increase with logarithm of loading rate (points in Fig. 4A). Higher strength of LFA-1-ICAM-1 bond was found in most cases except for the lowest loading rate (Fig. 4A), consistent with the dominate adhesion strength of LFA-1 in mediating fMLF-activated PMN adhesion on TNF-α-stimulated LSECs at cellular level [Yang, Li, Du et al. (2017)]. Fitting the loading rate dependence of mean force by a dynamic force spectroscopy theory [Eq. (3); Bell (1978); Evans and Ritchie (1997)] (lines in Fig. 4A) gave the Bell model parameters, k^0 and a (Tab. 1), for LFA-1- or Mac-1-ICAM-1 bond, respectively. The equilibrium dissociation rate k^0 was 0.034 s^{-1} for LFA-1 and 0.017 s^{-1} for Mac-1, suggesting a longer bond lifetime ($1/k^0$) for Mac-1 at zero-force. In order to compare the force-dependent lifetimes between LFA-1- and Mac-1-ICAM-1 bonds under external force, those rupture force histograms were directly transformed into the force dependence of bond lifetimes measurable in constant-force experiments by Eq. (4) (Fig. 4B) [Dudko, Hummer and Szabo (2008)], which also fitted the Bell model well, as expected (lines in Fig. 4B). The lifetime of LFA-1-ICAM-1 bonds was longer than those of Mac-1-ICAM-1 bonds under same pulling force, implying the slower dissociation of LFA-1-ICAM-1 bonds to support PMN firm adhesion. These results confirm the

observation at cellular level [Yang, Li, Du et al. (2017)], revealing the high strength and long lifetimes for LFA-1-ICAM-1 bonds to support PMN adhesion on LSECs under shear flow.

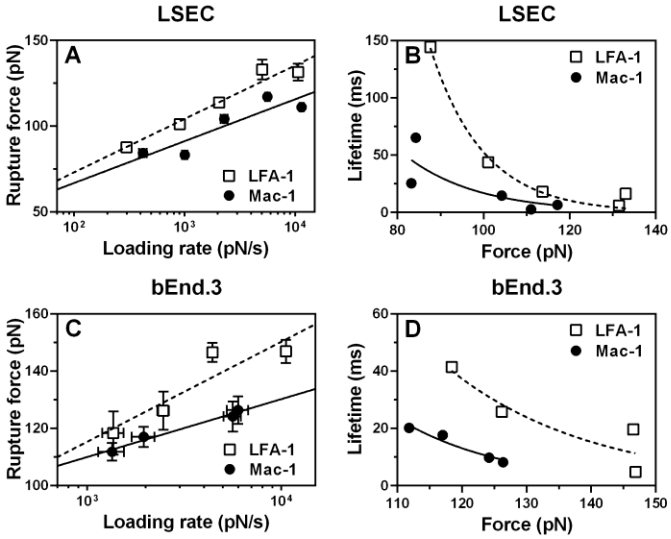

Figure 4: Rupture forces and lifetimes of the bonds between Mn^{2+}-activated LFA-1s (open squares, dashed lines) or Mac-1s (closed circles, solid lines) on the AFM cantilever tips and ICAM-1s expressed on TNF-α-stimulated LSECs (*A-B*) or LPS-stimulated bEnd.3 cells (*C-D*). (*A, C*) Dependence of rupture force on loading rate. Data are presented as the mean ± SEM of 36~144 force data at each loading rate and fitted by Eq. (3) (lines). (*B, D*) Lifetime (points) as a function of applied force, obtained from the variance of rupture force distribution using Eq. (4). The fitted curves (lines) were obtained using Eq. (1).

Table 1: Summary of Bell model parameters of LFA-1/Mac-1-ICAM-1 interactions

Integrin	Cell	k^0 (s^{-1})	a (Å)
LFA-1	LSEC	0.034	3.03
Mac-1	LSEC	0.017	3.87
LFA-1	bEnd.3	0.033	2.71
Mac-1	bEnd.3	0.0004	4.67

To further understand the tissue specificity of ICAM-1 binding strength to β_2 integrins, a distinct mouse cerebrovascular endothelial cell line bEnd.3 was applied as control group where PMN recruitment are assumed to follow the classical paradigm involving selectin-mediated rolling and β_2 integrin-dominated firm adhesion [Ley, Laudanna, Cybulsky et al. (2007); McDonald, McAvoy, Lam et al. (2008)]. Noting that the binding of LFA-1- or

Mac-1-coated tips to ICAM-1s on TNF-α-stimulated bEnd.3 cells was quite low (data not shown), a LPS stimulating model of bEnd.3 cells was instead used to produce the specific adhesive events and rupture forces of the interactions between β_2 integrin-ICAM-1 molecules. Rupture force of LFA-1-ICAM-1 binding was also higher than Mac-1-ICAM-1 binding under same loading rates on bEnd.3 cells (Fig. 4C) and the lifetime of LFA-1-ICAM-1 bonds was longer than those of Mac-1-ICAM-1 bonds under same external force (Fig. 4D), implying that LFA-1-ICAM-1 complex might play the dominant role in shear-resistant adhesion of PMNs compared with Mac-1-ICAM-1 complex on bEnd.3 cells. The zero-force dissociation rate k^0 was 0.033 s^{-1} for LFA-1 and 0.004 s^{-1} for Mac-1, suggesting that the spontaneous dissociation of Mac-1-ICAM-1 were slower than that for LFA-1. These data indicated that the differences between LFA-1- and Mac-1-ICAM-1 interactions seem irrelevant to tissue specificity, which may be attributed to their distinct conformations, as discussed below.

3.3 Structural basis of the binding of β_2-integrins to ICAM-1s

Force differences so observed in LFA-1- or Mac-1-ICAM-1 binding are assumed to correlate their distinct conformations. Here structural differences were compared using human LFA-1-I-domain *vs.* ICAM-1-D1-domain and Mac-1-I-domain *vs.* ICAM-1-D3-domain as the templates, since the LFA-1/Mac-1 I domain and ICAM-1 D1/D3 domain are the direct ligand-binding domains and no crystal structures have been found for murine ICAM-1-β_2-integrin complexes yet. Our previous MD analyses implied that the association of Mac-1 to ICAM-1 is much harder than that of LFA-1 since LFA-1-I-domain is able to bind spontaneously to ICAM-1 D1 domain but Mac-1-I-domain requires external force to bind effectively to ICAM-1 D3 domain due to shielding effect of side-chain of D229 residue in D3 domain by S142 and S144 in Mac-1 I domain [Li, Mao, Lü et al. (2013)]. From the viewpoint of bond dissociation, it was indicated here that total interacting energy between LFA-1/Mac-1 I-domain and ICAM-1 D1/D3 domain was higher for Mac-1 than that for LFA-1 (*black bars* in Fig. 5A). Further analysis of binding sites distribution illustrated two main sites on ICAM-1 side for each system. That is, E34 and Q73 residues of ICAM-1 D1 domain bound respectively to Ca^{2+} cation and N207 of LFA-1 I domain (Fig. 5B) that were consistent with the crystallized structure of LFA-1 I domain-ICAM-1 complex [Shimaoka, Xiao, Liu et al. (2003)] and experimental measurements [Bella, Kolatkar, Marlor et al. (1998)], while D229 and E254 of ICAM-1 D3 domain bound respectively to Ca^{2+} cation and H148 and R151 of Mac-1 I domain (Fig. 5C) that were in accordance with the measurements of the impact of D229 and E254 mutation on Mac-1-ICAM-1 interaction [Diamond, Staunton, Marlin et al. (1991)]. Specifically, the interaction energy between E34 in D1 domain or D229 in D3 domain and Ca^{2+} cation yielded more than 50% of total energy for both LFA-1 and Mac-1 systems (*white bars* in Fig. 5A). These results suggested that the spontaneous dissociation of Mac-1-I-domain *vs.* ICAM-D3-domain seemed slower with the stronger interaction energy than that for LFA-1.

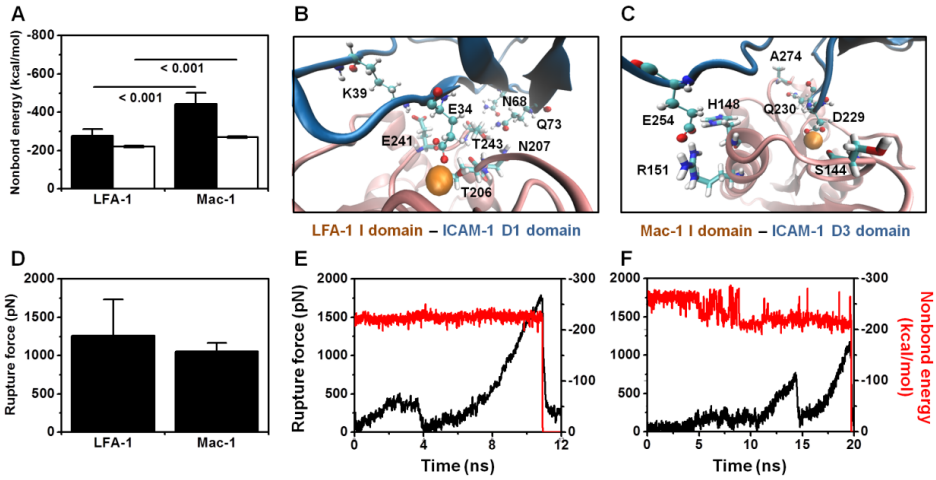

Figure 5: Microstructural basis of LFA-1-ICAM-1 and Mac-1-ICAM-1 interactions in both equilibration and forced dissociation simulations. (*A*, *B*, *C*) Nonbond interaction energy of global interaction between LFA-1/Mac-1 I domain and ICAM-1 D1/D3 domain (black bars) and of partial interaction between metal ion of LFA-1/Mac-1 I domain and E34/D229 of ICAM-1 D1/D3 domain (white bars) (*A*), and distribution of key binding sites for LFA-1 I domain-ICAM-1 D1 domain (*B*) and for Mac-1 I domain-ICAM-1 D3 domain (*C*) interactions in equilibration simulations. Nonbond interaction energy was presented as mean ±SD of the last 5-*ns* average of eleven and three runs for LFA-1-ICAM-1 and Mac-1-ICAM-1 systems, respectively. 10-*ns* snapshots of one typical equilibration run for LFA-1/Mac-1-ICAM-1 complex were presented in (*B*-*C*). Key residues involved in binding from LFA-1/Mac-1 I domain (pink cartoon) or ICAM-1 D1/D3 domain (blue cartoon) were shown as *Licorice* and *CPK*, respectively, and Ca^{2+} cation was presented as VDW. (*D*, *E*, *F*) Rupture force of complex dissociation under *cv*-steered MD of 0.01 Å/ps (*D*), and typical dissociation dynamics of force-time (*black*) and metal ion-key residue interaction-time (red) profiles for LFA-1-ICAM-1 (*E*) and Mac-1-ICAM-1 (*F*) systems. Rupture force was quantified as the maximum force around the moment for metal ion dissociation and presented as mean ±SD of seven and three independent runs for LFA-1-ICAM-1 and Mac-1-ICAM-1 systems, respectively

Under external force, however, the rupture force for Mac-1 was lower than that for LFA-1 (Fig. 5D). Evolution of a typical *cv*-steered MD forced unbinding process demonstrated that the release of cation from ligand was the key step of complex dissociation with the abrupt dropping of interaction energy between E34 in D1 domain or D229 in D3 domain and Ca^{2+} cation (red line), which was in synchronization with the maximum rupture force (black line) (Figs. 5E-5F). This finding suggested that the E34- or D229-Ca^{2+} cation interaction governed the rupture force. Although the D229-Ca^{2+} interaction energy in Mac-1-ICAM-1 complex was higher than the E34-Ca^{2+} interaction energy in LFA-1-ICAM-1 complex during equilibration simulation (white bars in Fig. 5A), the former was less stable with large fluctuation and gradual reduction under external force (red line in Fig. 5F) while the latter kept stable until complex dissociation (red line in Fig. 5E), resulting in the lower rupture force for Mac-1-ICAM-1 complex than that for LFA-1-

ICAM-1 complex (Fig. 5D). Collectively, these MD analyses are in qualitative agreement with the above experimental observations on the equilibrium dissociation and forced rupture between LFA-1- and Mac-1-ICAM-1 interactions (Tab. 1 and Fig. 4).

4 Discussion

PMNs adhesion on LSECs and extravasation into the parenchyma is crucial to pathogen clearance or tissue damage [Ramaiah and Jaeschke (2007); Kolaczkowska and Kubes (2013)]. While selectin-mediated PMN tethering and rolling unlikely appears in liver sinusoids due to the absence of selectins on LSECs, the binding of LFA-1 and Mac-1 to their ligands on LSECs has a pivotal role in supporting the recruitment of PMNs under shear flow [Menezes, Lee, Zhou et al. (2009); Yang, Li, Du et al. (2017)]. Here we quantified the mechanical strength binding LFA-1 or Mac-1 to ligands on LSECs at molecular level and revealed a dominate role for LFA-1.

The first step required for testing LFA-1 and Mac-1 binding on LSECs is to obtain undifferentiated primary cells. It is well known that isolated primary LSECs quickly lose their phenotype out of their *in vivo* environment. In current work, we used AFM to image LSEC ultrastructure and confirmed that the fenestration phenotype could be maintained well within experimental duration (Fig. 1). Traditional fenestration imaging using scanning electron microscope (SEM) [Wisse, Zanger, Jacobs et al. (1983)] requires the samples fixed by glutaraldehyde-osmium tetroxide, dehydrated, dried at critical point, and coated with a thin layer of gold. This complicated preparatory process may cause the structural damage and even create the additional holes on cell surface [Braeta and Wissea (2012); Poisson, Lemoinne, Boulanger et al. (2017)]. In the current work, the AFM imaging only need the samples to be fixed by glutaraldehyde, reserving the valid information for fenestra at the greatest degree.

The adhesion of fMLF-activated PMNs on TNF-α-stimulated LSECs is mediated by the interactions between β_2 integrins on PMNs and their ligand ICAM-1 on LSECs [Menezes, Lee, Zhou et al. (2009); Yang, Li, Du et al. (2017)]. Mechanical force imposed by blood flow is an important factor to regulate the formation and dissociation of β_2-integrin and ICAM-1 bonds [Feng, Lee and Lim (2017)]. While a body of experimental evidences and theoretical predictions has been reported to elucidate the mechanistic insights of rupture force and energy landscape for forced dissociation of β_2-integrin-ICAM-1 bond [Wojcikiewicz, Abdulreda, Zhang et al. (2006); Yang, Yu, Fu et al. (2007); Chen, Lou and Zhu (2010); Evans, Kinoshita, Simon et al. (2010); Kinoshita, Leung, Simon et al. (2010); Celik, Faridi, Kumar et al. (2013)], this work first tested the rupture force of reconstructed LFA-1s or Mac-1s immobilized on a AFM cantilever tip to ICAM-1s anchored onto a LSEC cell. Our data indicated that the higher rupture force was observed for binding of hepatic ICAM-1 to LFA-1 than that to Mac-1 (Fig. 4A), consistent with our steered MD analysis (Fig. 5D) and the shear-resistant data in our previous work [Li, Yang, Wang et al. (2018)]. Taken together, these results suggest that LFA-1 appears to be more important in PMN adhesion on LSECs *in vitro*, which is similar with data from postcapillary venules or purified recombinant proteins but not consistent with previous *in vivo* works [Ding, Babensee, Simon et al. (1999); McDonald, McAvoy, Lam et al. (2008); Menezes, Lee, Zhou et al. (2009); McDonald, Pittman, Menezes et al. (2010); Jenne,

Wong, Zemp et al. (2013); Robert, Brechtefeld and Walzog (2013); Li, Yang, Wang et al. (2018)]. It is notable that the liver sinusoids have specialized narrow luminal diameter (d=7-15 μm) and slow blood flow (τ_w=0.1-1 dyn/cm^2), potentiating a great impact on PMN recruitment [McDonald, McAvoy, Lam et al. (2008)]. The force (=$32\tau_w r^2$) applied to mouse PMNs by physiological shear flow in the liver sinusoids is estimated to be 8-80 pN (the radius r is calculated as 4 μm) [McEver and Zhu (2010)]. Therefore both LFA-1 and Mac-1 could resist the quite low mechanical force applied by slow blood flow in the liver sinusoids. Together with the 10-fold higher molecular density of Mac-1 than that of LFA-1 on fMLF-activated PMNs [Yang, Li, Du et al. (2017)], the effects of Mac-1 may outdo LFA-1 *in vivo* [Menezes, Lee, Zhou et al. (2009)].

5 Conclusion

We investigated the mechanical strength binding LFA-1 or Mac-1 to ICAM-1 on LSECs using AFM tests and MD simulations and proposed a dominate role for LFA-1 to mediate shear-resistant adhesion, indicating that the biomechanical features of LFA-1 and Mac-1 to mediate PMN adhesion on LSECs *in vitro* are similar with that in other tissues like cerebrovascular endothelium. Those Mac-1-controled PMN recruitment *in vivo* in the sinusoids may stem from the slow blood flow in liver sinusoids. This work bridges the gap between mechanical strength through LFA-1s or Mac-1s and their biological functions in cell adhesion under shear flow, providing an insight into understanding the mechanisms of distinct PMN recruitment paradigm in liver.

Acknowledgement: This work was supported by National Key Research and Development Program of China Grant 2016YFA0501601, National Natural Science Foundation of China Grants 31661143044, and 31300776, Strategic Priority Research Program and Frontier Science Key Project of Chinese Academy of Sciences Grants XDB22040101 and QYZDJ-SSW-JSC018 and the Visiting Scholar Foundation of the Key Laboratory of Biorheological Science and Technology (Chongqing University), Ministry of Education (CQKLBST-2015-002).

Conflict of interest statement: The authors declare neither conflict of interest nor competing financial interest.

References

Bella, J.; Kolatkar, P. R.; Marlor, C. W.; Greve, J. M.; Rossmann, M. G. (1998): The structure of the two amino-terminal domains of human ICAM-1 suggests how it functions as a rhinovirus receptor and as an LFA-1 integrin ligand. *Proceedings of the National Academy of Sciences of the United States of America*, vol. 95, no. 8, pp. 4140-4145.

Bell, G. I. (1978): Models for specific adhesion of cells to cells. *Science*, vol. 200, pp. 618-627.

Braet, F.; Shleper, M.; Paizi, M; Brodsky, S.; Kopeiko, N. et al. (2004): Liver sinusoidal endothelial cell modulation upon resection and shear stress *in vitro*. *Comparative Hepatology*, vol. 3, no. 1-7.

Braet, F.; Wissea, E. (2012): AFM imaging of fenestrated liver sinusoidal endothelial cells. *Micron*, vol. 43, pp. 1252-1258.

Celik, E.; Faridi, M. H.; Kumar, V.; Deep, S.; Moy, V. T. et al. (2013): Agonist leukadherin-1 increases CD11b/CD18-dependent adhesion via membrane tethers. *Biophysical Journal*, vol. 105, no. 11, pp. 2517-2527.

Chen, W.; Lou, J. Z.; Zhu, C. (2010): Forcing switch from short- to intermediate- and long-lived states of the alpha A domain generates LFA-1/ICAM-1 catch bonds. *Journal of Biological Chemistry*, vol. 285, no. 46, pp. 35967-35978.

Diamond, M. S.; Staunton, D. E.; Marlin, S. D.; Springer, T. A. (1991): Binding of the integrin Mac-1 (CD11b/CD18) to the third immunoglobulin-like domain of ICAM-1 (CD54) and its regulation by glycosylation. *Cell*, vol. 65, no. 6, pp. 961-971.

Ding, Z. M.; Babensee, J. E.; Simon, S. I; Lu, H. F.; Jerry, L. et al. (1999): Relative contribution of LFA-1 and Mac-1 to neutrophil adhesion and migration. *Journal of Immunology*, vol. 163, pp. 5029-5038.

Du, Y.; Li, N.; Yang, H.; Luo, C. H.; Gong, Y. X. et al. (2017): Mimicking liver sinusoidal structures and functions using a 3D-configured microfluidic chip. *Lab on a Chip*, vol. 17, no. 5, pp. 782-794.

Dudko, O. K.; Hummer, G.; Szabo, A. (2008): Theory, analysis, and interpretation of single-molecule force spectroscopy experiments. *Proceedings of the National Academy of Sciences of the United States of America*, vol. 105, pp. 15755-15760.

Evans, E.; Kinoshita, K.; Simon, S.; Leung, A. (2010): Long-lived, high-strength states of ICAM-1 bonds to β_2 integrin, I: Lifetimes of bonds to recombinant $\alpha_L\beta_2$ under force. *Biophysical Journal*, vol. 98, pp. 1458-1466.

Evans, E.; Ritchie, K. (1997): Dynamic strength of molecular adhesion bonds. *Biophysical Journal*, vol. 72, pp. 1541-1555.

Feng, X. Q.; Lee, P. V. S.; Lim, C. T. (2017): Preface: Molecular, cellular, and tissue mechanobiology. *Acta Mechanica Sinica*, vol. 33, no. 2, pp. 219-221.

Ford, A. J.; Jain, G.; Rajagopalan, P. (2015): Designing a fibrotic microenvironment to investigate changes in human liver sinusoidal endothelial cell function. *Acta Biomaterialia*, vol. 24, pp. 220-227.

Heymann, F.; Tacke, F. (2016): Immunology in the liver-from homeostasis to disease. *Nature Reviews Gastroenterology & Hepatology*, vol. 13, pp. 88-110.

Humphrey, W.; Dalke, A.; Schulten, K. (1996): VMD: Visual molecular dynamics. *Journal of Molecular Graphics & Modelling*, vol. 14, no. 1, pp. 33-38.

Ito, Y.; Abril, E. R; Bethea, N. W.; McCuskey, M. K.; Cover, C. et al. (2006): Mechanisms and pathophysiological implications of sinusoidal endothelial cell gap formation following treatment with galactosamine/endotoxin in mice. *American Journal of Physiology-Gastrointestinal and Liver Physiology*, vol. 291, no. 2, pp. 211-218.

Jenne, C. N.; Wong, C. H. Y.; Zemp, F. J.; McDonald, B.; Rahman, M. et al. (2013): Neutrophils recruited to sites of infection protect from virus challenge by releasing neutrophil extracellular traps. *Cell Host & Microbe*, vol. 13, no. 2, pp. 169-180.

Juin, A.; Planus, E.; Guillemot, F.; Horakova, P.; Albiges-Rizo, C. et al. (2013): Extracellular matrix rigidity controls podosome induction in microvascular endothelial cells. *Biology of the Cell*, vol. 105, no. 1, pp. 46-57.

Kinoshita, K.; Leung, A.; Simon, S.; Evans, E. (2010): Long-lived, high-strength states of ICAM-1 bonds to β_2 integrin, II: Lifetimes of LFA-1 bonds under force in leukocyte signaling. *Biophysical Journal*, vol. 98, pp. 1467-1475.

Kolaczkowska, E.; Kubes, P. (2013): Neutrophil recruitment and function in health and inflammation. *Nature Reviews Immunology*, vol. 13, no. 3, pp. 159-175.

Ley, K.; Laudanna, C.; Cybulsky, M. I.; Nourshargh, S. (2007): Getting to the site of inflammation: The leukocyte adhesion cascade updated. *Nature Reviews Immunology*, vol. 7, pp. 678-689.

Li, N.; Mao, D. B.; Lü, S. Q.; Tong, C. F.; Zhang, Y. et al. (2013): Distinct binding affinities of Mac-1 and LFA-1 in neutrophil activation. *Journal of Immunology*, vol. 190, no. 8, pp. 4371-4381.

Li, N.; Yang, H.; Wang, M. L.; Lü, S. Q.; Zhang, Y. et al. (2018): Ligand-specific binding forces of LFA-1 and Mac-1 in neutrophil adhesion and crawling. *Molecular Biology of the Cell*, vol. 29, no. 4, pp. 408-418.

Lu, C.; Shimaoka, M.; Ferzly, M.; Oxvig, C.; Takagi, J. et al. (2001): An isolated, surface-expressed I domain of the integrin αLβ2 is sufficient for strong adhesive function when locked in the open conformation with a disulfide bond. *Proceedings of the National Academy of Sciences of the United States of America*, vol. 98, no. 5, pp. 2387-2392.

Lü, S. Q.; Long, M. (2005): Forced dissociation of selectin-ligand complexes using steered molecular dynamics simulation. *Molecular & Cellular Biomechanics*, vol. 2, no. 4, pp. 161-177.

Lü, S. Q.; Ye, Z. Y.; Zhu, C.; Long, M. (2006): Quantifying the effects of contact duration, loading rate, and approach velocity on P-selectin-PSGL-1 interactions using AFM. *Polymer*, vol. 47, pp. 2539-2547.

Lyck, R.; Enzmann, G. (2015): The physiological roles of ICAM-1 and ICAM-2 in neutrophil migration into tissues. *Current Opinion in Hematology*, vol. 22, pp. 53-59.

Mao, D. B.; Lü, S. Q.; Li, N.; Zhang, Y.; Long, M. (2011): Conformational stability analyses of alpha subunit I domain of LFA-1 and Mac-1. *PLoS One*, vol. 6, no. 8.

MacKerell, A. D.; Bashford, D.; Bellott, M.; Dunbrack, R. L.; Evanseck, J. D. et al. (1998): All-atom empirical potential for molecular modeling and dynamics studies of proteins. *Journal of Physical Chemistry B*, vol. 102, no. 18, pp. 3586-3616.

McDonald, B.; McAvoy, E. F.; Lam, F.; Gill, V.; de la Motte, C. et al. (2008): Interaction of CD44 and hyaluronan is the dominant mechanism for neutrophil sequestration in inflamed liver sinusoids. *Journal of Experimental Medicine*, vol. 205, pp. 915-927.

McDonald, B.; Pittman, K.; Menezes, G. B.; Hirota, S. A.; Slaba, I. et al. (2010): Intravascular danger signals guide neutrophils to sites of sterile inflammation. *Science*, vol. 330, no. 6002, pp. 362-366.

McEver, R. P.; Zhu, C. (2010): Rolling cell adhesion. *Annual Review of Cell and*

Developmental Biology, vol. 26, pp. 363-396.

Menezes, G. B.; Lee, W.-Y.; Zhou, H.; Waterhouse, C. C. M.; Cara, D. C. et al (2009): Selective down-regulation of neutrophil Mac-1 in endotoxemic hepatic microcirculation via IL-10. *The Journal of Immunology*, vol. 183, pp. 7557-7568.

Mittal, S.; Dwivedi, A. (2017): Local and biglobal linear stability analysis of parallel shear flows. *Computer Modeling in Engineering & Sciences*, vol. 113, no. 2, pp. 219-237.

Phillips, J. C.; Braun, R.; Wang, W.; Gumbart, J.; Tajkhorshid, E. et al. (2005): Scalable molecular dynamics with NAMD. *Journal of Computational Chemistry*, vol. 26, no. 16, pp. 1781-1802.

Poisson, J.; Lemoinne, S.; Boulanger, C.; Durand, F.; Moreau, R. et al. (2017): Liver sinusoidal endothelial cells: Physiology and role in liver diseases. *Journal of Hepatology*, vol. 66, no. 1, pp. 212-227.

Ramaiah, S. K.; Jaeschke, H. (2007): Role of neutrophils in the pathogenesis of acute inflammatory liver injury. *Toxicologic Pathology*, vol. 35, pp. 757-766.

Robert, P.; Brechtefeld, D.; Walzog, B. (2013): Intraluminal crawling versus interstitial neutrophil migration during inflammation. *Molecular Immunology*, vol. 55, no. 1, pp. 70-75.

Sanabria, V. A.; Dong, C. (2018): Integration of biochemical and biomechanical signals regulating endothelial barrier function. *Molecular & Cellular Biomechanics*, vol. 15, no. 1, pp. 1-19.

Shimaoka, M.; Lu, C.; Salas, A.; Xiao, T.; Takagi, J. et al. (2002): Stabilizing the integrin αM inserted domain in alternative conformations with a range of engineered disulfide bonds. *Proceedings of the National Academy of Sciences of the United States of America*, vol. 99, no. 26, pp. 16737-16741.

Shimaoka, M.; Xiao, T.; Liu, J. H.; Yang, Y.; Dong, Y. et al. (2003): Structures of the alpha L I domain and its complex with ICAM-1 reveal a shape-shifting pathway for integrin regulation. *Cell*, vol. 112, no. 1, pp. 99-111.

Shi, J. Y.; Wang, F.; Liu, S. (2016): Radiolabeled cyclic RGD peptides as radiotracers for tumor imaging. *Biophysics Reports*, vol. 2, no. 1, pp. 1-20.

Swartjes, J. J. T. M.; Veeregowda, D. H. (2015): Implications for directionality of nanoscale forces in bacterial attachment. *Biophysics Reports*, vol. 1, no. 3, pp. 120-126.

Yang, H.; Yu, J.; Fu, G.; Shi, X.; Xiao, L. et al. (2007): Interaction between single molecules of Mac-1 and ICAM-1 in living cells: An atomic force microscopy study. *Experimental Cell Research*, vol. 313, no. 16, pp. 3497-3504.

Tees, D. F. J.; Waugh, R. E.; Hammer, D. A. (2001): A microcantilever device to assess the effect of force on the lifetime of selectin-carbohydrate bonds. *Biophysical Journal*, vol. 80, pp. 668-682.

Vollmar, B.; Menger, M. D. (2009): The hepatic microcirculation: mechanistic contributions and therapeutic targets in liver injury and repair. *Physiological Reviews*, vol. 89, pp. 1269-1339.

Wisse, E.; De Zanger, R. B.; Jacobs, R.; McCuskey, R. S. (1983): Scanning electron microscope observations on the structure of portal veins, sinusoids and central veins in rat liver. *Scanning Electron Microscopy*, vol. 3, pp. 1441-1452.

Wojcikiewicz, E. P.; Abdulreda, M. H.; Zhang, X.; Moy, V. T. (2006): Force spectroscopy of LFA-1 and its ligands, ICAM-1 and ICAM-2. *Biomacromolecules*, vol. 7, no. 11, pp. 3188-3195.

Xu, M. X; Wang, X. H.; Zou, Y.; Zhong, Y. S. (2017): Key role of liver sinusoidal endothelial cells in liver fibrosis. *BioScience Trends*, vol. 11, no. 2, pp. 163-168.

Yamasaki, M.; Ikeda, K.; Nakatani, K.; Yamamoto, T.; Kawai, Y. et al. (1999): Phenotypical and morphological alterations to rat sinusoidal endothelial cells in arterialized livers after portal branch ligation. *Archives of Histology and Cytology*, vol. 62, no. 5, pp. 401-411.

Yang, H.; Li, N.; Du, Y.; Tong, C. F.; Lü, S. Q. et al. (2017): Neutrophil adhesion and crawling dynamics on liver sinusoidal endothelial cells under shear flow. *Experimental Cell Research*, vol. 351, no. 1, pp. 91-99.

Zapotocznya, B.; Szafranskaa, K.; Kusb, E.; Chlopickib, S.; Szymonskia, M. (2017): Quantification of fenestrations in liver sinusoidal endothelial cells by atomic force microscopy. *Micron*, vol. 101, pp. 48-53.

Zhang, X.; Wojcikiewicz, E.; Moy V. T. (2002): Force spectroscopy of the leukocyte function-associated antigen-1/intercellular adhesion molecule-1 interaction. *Biophysical Journal*, vol. 83, no. 4, pp. 2270-2279.

Zhang, Y.; Sun, G. Y.; Lü, S. Q.; Li, N.; Long, M. (2008): Low spring constant regulates P-selectin-PSGL-1 bond rupture. *Biophysical Journal*, vol. 95, pp. 5439-5488.